Investigation of Optical Material Removal Characteristics Using Ion Sputtering

Zuocai Dai[1,a,*] and Tongguang Yang[1,b]

[1]*School of Mechanical and Electrical Engineering, Hunan City University, China*
a. daizuocai@163.com, b. 13387371899@139.com
**corresponding author: Zuocai Dai*

Keywords: Material removal characteristics, ion beam processing, sputtering yield.

Abstract: The removal performance of optical materials by ion beam sputtering is investigated in this paper. the bombardment process of Ar+ and Kr+ was simulated through the software TRIM. It is feasible to achieve a high removal rate by using Ar+ ion beam with a big incident angle, which demonstrates that the material removal sputtering yield rises up with the increase of the incident ion energy and incident angle within a certain range. The material removal principle is of great significance to the further performance application of the ion processing in the field of optical processing.

1. Introduction

Ion beam processing technology has become the last process commonly used in the ultra-precision processing of optical materials. The material removal at the atomic level can realize the sub-nanometre processing accuracy of ion beam processing[1,2]. The core of the ion beam processing system is the ion sputtering. The performance of the ion energy state directly determines the processing ability of the ion beam system[3].

Ion beam processing is more advanced than the traditional optical processing methods for non-contact stress and subsurface damage on the processed optical surface. According to the Sigmund sputtering theory, energy and momentum transfer from the incident ions to the substrate atoms due to the collision[4]. If the collided atoms obtain enough energy to break off the crystal lattice bound, they will bombard the other atoms together with the incident ions[5,6]. In these collisions, the atoms on the surface will fly off when they obtain enough energy to overcome the surface bound. This physical phenomenon is named sputtering effect.

In this paper, In order to explore the methods to enhance the ion beam removal rate through the sputtering effect, the removal performance of optical materials by ion beam sputtering is investigated. the bombardment process of Ar+ and Kr+ had been simulated through the software TRIM, and the sputtering yield was calculated. It is feasible to achieve a high removal rate by using Kr+ ion beam with a big incident angle. The material removal principle and good stability are of great significance to the further performance application of the ion processing in the field of optical processing.

2. Material Removal Mechanism

The material removal characteristics during the ion beam processing are the spatial distribution of the material removal rate of the work-piece under the action of the ion beam processing. The properties that the material removal characteristics can be closely related to the principle of material removal rate. Ion beam processing uses the ion sputtering effect to remove the work-piece material. During the ion beam processing process, There is not only the ion sputtering effect, but also a chemical reaction in the reactive ion beam processing[3]. The material removal distribution is not only closely related to the properties of the work-piece material, ion beam current, and angle of incidence, but also to the chemical reaction rate, temperature, and ion concentration of the reactive ion beam. Based on the Sigmund sputtering mechanism, firstly, the theoretical model of the material removal mechanism of physical sputtering for ion beam processing is analyzed, and various characteristics of the material removal process is investigated.

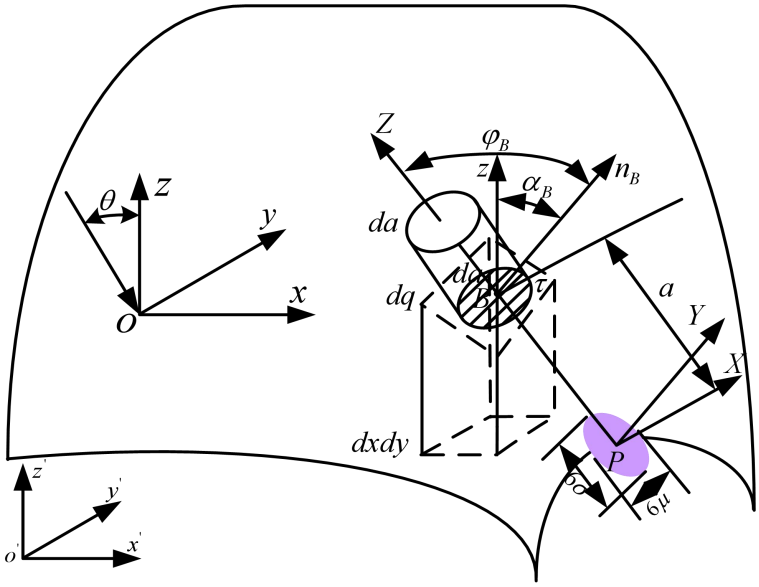

Figure 1: Schematic diagram of normal material removal mechanism.

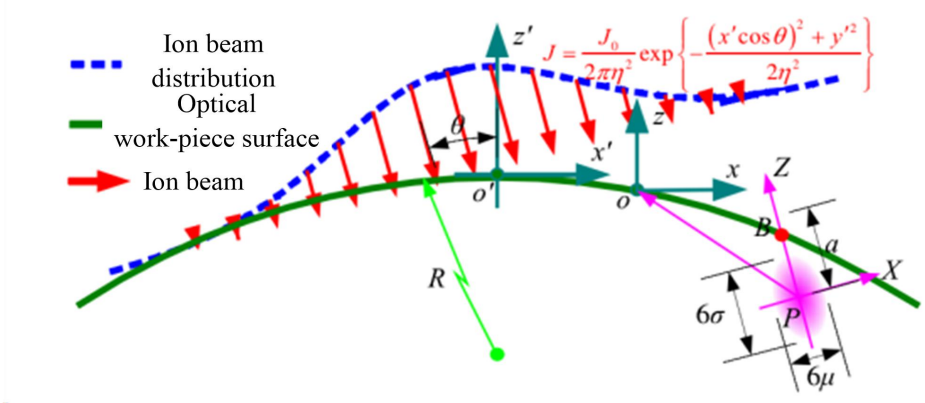

Figure 2: Material removal principle of optical spherical surface under Gaussian ion beam.

Figure 1 shows the normal removal mechanism. When the Gaussian ion beam acts on the optical surface, the X, Y, and Z axes of the energy scattering coordinate system at point B are expressed as

the work-piece reference coordinate system. According to the definition of the coordinate system, the X, Y, and Z axes of $o-xyz$ can be described as

$$\begin{cases} \mathrm{X}=[\cos\theta \quad 0 \quad \sin\theta] \\ Y=[0 \quad 1 \quad 0] \\ Z=[-\sin\theta \quad 0 \quad \cos\theta] \end{cases} \tag{1}$$

The energy scattering center P at point B on the work-piece is expressed as

$$p=\left[x-a\sin\theta \quad y \quad z-a\cos\theta\right] \tag{2}$$

The coordinates in the coordinate system of the energy scattering center O are obtained as

$$O_{P-XYZ}=\left[-x\cos\theta+z\sin\theta \quad -y \quad -x\sin\theta-z\cos\theta+\mathrm{a}\right] \tag{3}$$

It is assumed that the surface of the work-piece can be represented by a continuous function $h(x,y)$ in coordinates $o-xyz$. The minimum radius of curvature of the surface at any point is much larger than the average energy scattering depth a, and can be expanded into the area of o:

$$h(x,y)=\frac{\partial h}{\partial x}x+\frac{\partial h}{\partial y}y+\frac{1}{2}\frac{\partial^2 h}{\partial x^2}x^2+\frac{\partial^2 h}{\partial x\partial y}xy+\frac{1}{2}\frac{\partial^2 h}{\partial y^2}y^2 \tag{4}$$

As shown in Figure 1, n_B is the outer normal at point B and φ_{B} is the angle between n_B and the Z axis. The local correction function of the beam density introduced by the tilt angle is

$$\phi=J\cos\varphi_B=\frac{J(x,y,z)(\cos\theta-\frac{\partial h}{\partial x}\big|_B\sin\theta)}{\sqrt{1+(\frac{\partial h}{\partial x}\big|_B)^2+(\frac{\partial h}{\partial y}\big|_B)^2}} \tag{5}$$

Where, α_{B} is the angle between n_B and the Z axis, J is Gaussian beam density. According to the calculus theory, the specific expression of the surface area micro-element at the point B of the optical surface can be processed in the coordinate system, which can be described as

$$dq=\frac{dxdy}{\cos\alpha_B}=dxdy\sqrt{1+(\frac{\partial h}{\partial x}\big|_{\mathrm{B}})^2+(\frac{\partial h}{\partial y}\big|_{\mathrm{B}})^2} \tag{6}$$

The normal material removal rate at point o is solved in the work-piece reference frame,which can be described as

$$
\begin{aligned}
v_o &= p\int \phi E \exp(-b(\cos^{-1}\varphi_B - 1))dq \\
&= \frac{p\varepsilon}{(2\pi)^{3/2}\sigma\mu^2}\int J(\cos\theta - \frac{\partial h}{\partial x}\big|_B \sin\theta)\exp(-b(\cos^{-1}\varphi_B - 1))\times \\
&\quad \exp(-\frac{(-x\sin\theta - z\cos\theta + a)^2}{2\sigma^2} - \frac{(-x\cos\theta + z\sin\theta)^2 + (-y)^2}{})dxdy
\end{aligned} \tag{7}
$$

If the incident angle is small, the first-order approximation of the formula $h(x,y)$ is

$$
\begin{aligned}
v_o = \frac{p\varepsilon}{(2\pi)^{3/2}\sigma\mu^2}\int J(\cos\theta - \frac{\partial h}{\partial x}\big|_{\mathrm{B}}\sin\theta)\exp(-(\frac{\sin^2\theta}{2\sigma^2} + \frac{\cos^2\theta}{2\mu^2})x^2)\exp(\frac{a\sin\theta}{\sigma^2}x)\times \\
\exp(-\frac{y^2}{2\mu^2})(1 + (\frac{x\sin 2\theta}{2\mu^2} + \frac{a\cos\theta}{\sigma^2} - \frac{x\sin 2\theta}{2\sigma^2})h(x,y))\,dxdy
\end{aligned} \tag{8}
$$

Where, ε indicates the total deposited energy, σ and μ is the Gaussian distribution parameters.

As shown in Fig. 2, assuming the work-piece is an ideal spherical surface, it can be approximately expressed in the work-piece reference coordinate $o'-x'y'z'$ system, and the formula $h(x,y)$ can be described as

$$
h(x,y) = -\frac{1}{2R}(x^2 + y^2) \tag{9}
$$

Where R is the radius of curvature. The axis of rotation symmetry of the incident Gaussian beam passes through the apex of the spherical surface, and within the plane $o'x'z'$, and θ is the angle between the z' axis and the the incident Gaussian beam. The beam density distribution in the medium can be described as

$$
J(x^{'},y^{'}) = \frac{J_0}{2\pi\eta^2}\exp(-\frac{(x^{'}\cos\theta)^2 + y^{'2}}{2\eta^2}) \tag{10}
$$

The beam density distribution width parameter η is generally millimeters. The material removal function can be obtained by the integral of the equation (10):

$$
\begin{aligned}
v_{gs}(x^{'},y^{'}) &= g_0 + g_x\partial_x h\big|_o + g_y\partial_y h\big|_o + g_{2x}\partial_x^2 h\big|_o + g_{2y}\partial_y^2 h\big|_o \\
&\approx g_0(1 - e_{gs}^{\mathrm{R}})
\end{aligned} \tag{11}
$$

Where

$$
g_0 \approx J(x^{'},y^{'})F\cos\theta \qquad e_{gs}^{R} = \frac{(a_\sigma^4 - a_\sigma^2)x^{'}\theta}{Ra_u^2}
$$

$$
F = \frac{\varepsilon p a_\mu a_\sigma}{a\sqrt{2\pi f}}\exp(-\frac{a_\sigma^2 a_\mu^2\cos^2\theta}{2f}) \qquad f = a_\sigma^2\sin^2\theta + a_\mu^2\cos^2\theta
$$

g_0 is the material removal function of the plane under the action of Gaussian beam. Considering the curvature radius R, and the width η of the removal function on the work-piece are much larger

than the sputtering parameters a, μ , σ in the sub-micron category[4,5]. when a unit uniform beam acts on the plane, the material removal function can be regarded as the product of the beam density distribution function $J(x', y')$ and the removal rate $F\cos\theta$. g_x , g_y , g_{2x} ,and g_{2y} are functions of the incidence angle θ.

The surface shape at any point o in the ion beam bombardment area can be expressed as

$$h(x, y) = 0 \qquad (12)$$

Substituting the equation (12) into the equation (9), it can be solved that the removal function of a uniform beam with a small angle of inclined incident plane. then, the removal function can be described as

$$v_{up} = JF\cos\theta \qquad (13)$$

As shown in equation (13), the removal function of the plane under a uniform beam is also uniform and proportional to the beam density.

3. Simulation

According to the material removal theoretical model of sputtering yield, the sputtering yield of incident ions is related to the ion energy deposition parameters and the incident angle. In ion beam optical processing applications, argon ions have the same mass as silicon atoms, and are widely used as working medium gases. The method of increasing the ion beam energy or increasing the incident angle to obtain high removal efficiency has been widely used. we mainly study the effect of ion type on sputtering yield. Taking into account the physical properties of the gas, we selected thorium ions for research. Krypton ions and argon ions have similar atomic radii and gas discharge characteristics, but have an atomic mass equivalent to twice that of argon ions, as shown in Table 1.

Table 1: Atomic parameters.

Atom	Relative atomic mass	Atomic radius (Å)	First ionization potential (V)	Electronic temperature (eV)
Ar	39.948	0.88	15.76	4～7
Kr	83.8	1.03	13.93	5～7

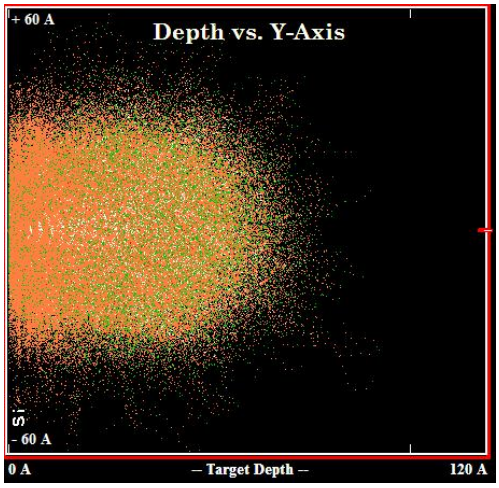

Figure 3: Simulation of argon ion deposition on the surface of single crystal silicon.

Even if the two incident ions have the same energy, the difference in mass and volume will lead to different energy deposition on the solid surface. We use the simulation software SRIM (Stopping and Range of Ions in Matter) The energy deposition on the silicon surface is simulated. SRIM uses the Monte Carlo method to calculate the transport of ions in a substance. It can give a good simulation result for a variety of ionic transport related phenomena such as range, energy loss, sputtering, and damage. We use the sputtering model for simulation. The simulation example is shown in Figure 3.

The incident ions used in the simulation are argon ions and krypton ions, the target material is single crystal silicon, and the simulated ion energy is 600 to 1100 eV. In normal incidence, the ion energy deposition parameters a, μ, and σ are shown in Figure 4.

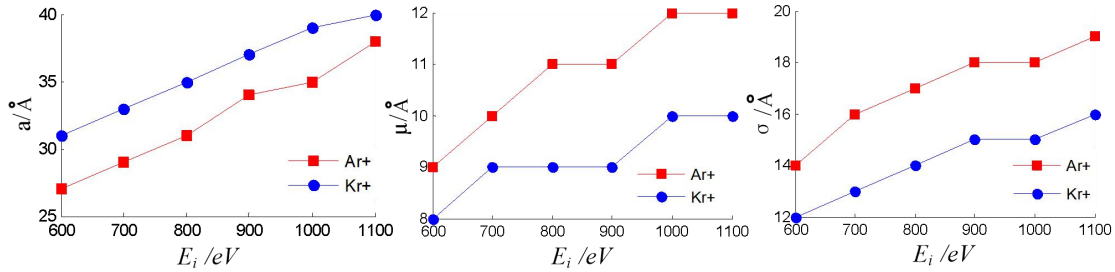

Figure 4: Simulation results of argon and krypton energy deposition parameters under normal incidence.

As the simulation results shown in Figure 4, it can be seen that for both ions, the energy deposition depth a increases with the increase of the ion energy, and the energy deposition parameters μ and σ along the perpendicular and parallel to the ion incidence direction follow the ion. Increasing incident energy increases, which is a common feature of the energy distribution of the two incident ions. Figure 5 is a graph showing the energy deposition distribution of two kinds of 1000 eV argon ions and krypton ions on the surface of single crystal silicon.

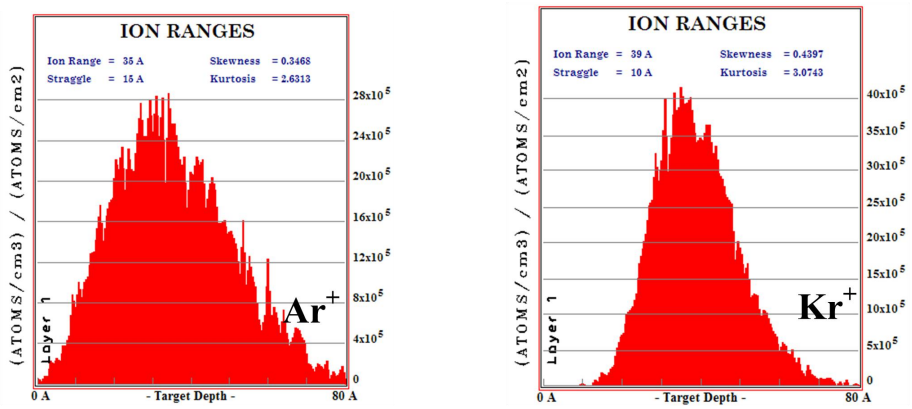

Figure 5: Energy distribution of ion deposition.

However, From the simulation results of the two kinds of ions at different energies in Figure 5, under the normal incidence conditions, the energy deposition depth of argon ions is always smaller than the energy deposition depth of erbium ions, and the argon ion incidence σ and μ are always greater than erbium ions. The deposition depth of the incident ion energy reflects the implantation depth of the ions on the solid surface. The above results show that under the normal incidence of more erbium ions implanted into the solid surface, the implantation of erbium ions will cause more deep atomic vibration. According to Figure 4, compared with the surface atoms, the deep-vibrating atoms are more difficult to overcome the layer-by-layer restraints from the solid surface, and most of the energy obtained by the deep-layer atoms in the collision will be consumed in the form of heat. μ and σ reflect the breadth of vibrating atoms caused by incident ions. The larger μ and σ means that the larger range of atoms are activated, which can achieve a larger sputtering yield. According to the simulation results in Figure 5, relative to the rubidium ions of the same energy, the argon ions can promote the vibration of the solid atoms in the surface layer in a larger range, and the energy deposition of the rubidium ions is relatively deep and concentrated. Therefore, under the normal incidence, argon ions with the same energy can achieve greater sputtering yield than krypton ions. The sputtering yield simulation results in Figure 6 confirm the correctness of the above analysis. It is worth noting that for certain incident ions, the energy deposition depth increases with the increase of ion energy, which is not conducive to the increase of ion sputtering yield. However, as the ion energy increases, σ and μ also increase at the same time, which makes up for the negative impact of increased energy deposition depth on sputtering yield. The results show that the yield of ion sputtering still increases with the increase of ion energy.

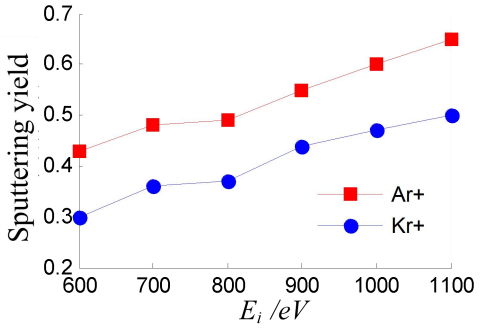

Figure 6: Simulation of argon ions and krypton ions in normal incidence sputtering yield.

According to the simulation results, because of the deep and concentrated energy deposition of the incident krypton ions, the surface atoms of mono-crystalline silicon can not be effectively activated to leave the surface. Under the condition of vertical incidence, more incident energy of krypton will be absorbed by mono-crystalline silicon in the form of heat. Therefore, for the small aperture focused ion optical system, krypton ions can not improve the removal efficiency of ion beam,while the removal efficiency will decrease.

4. Conclusions

The removal performance of optical materials by ion beam sputtering is investigated. the bombardment process of Ar+ and Kr+ had been simulated through the software TRIM. It is feasible to achieve a high removal rate by using Ar+ ion beam sputtering, the material removal sputtering yield of the mono-crystalline silicon material rises up with the increase of the incident ion energy within a certain range. The material removal principle is of great significance to the further performance application of the ion processing in the field of optical processing.

References

[1] A.I. Ayesh, Size-selected fabrication of alloy nanoclusters by plasma-gas condensation, Journal of Alloys and Compounds, (2018) 745.

[2] M. Chen,J. Wang,C.Q. Chen, and Z. Liu, Calculation and analysis based on Sigmund's theory for sputtering yield,VACUUM,(2007) 44(2) 44-47.

[3] R. Schelfhout, K. Strijckmans, D. Depla, Anomalous effects in the aluminum oxide sputtering yield, (2018) 51(15).

[4] D. Field, P.W. May, G.P.D. Forets, Sputtering of the refractory cores of interstellar grains, (2018) 285(4) 839-846.

[5] M. Benguerba, A model for sputtering from solid surfaces bombarded by energetic clusters, Nuclear Instruments and Methods in Physics Research, (2018) 420 27-32.

[6] C. Karapepas, D. Nestler, G. Wagner, Influence of Sputtering Temperature and Layer Thickness on the Electrical Performance of Thin Film Strain Sensors Consisting of Nickel-Carbon Composite, Key Engineering Materials, (2019) 809 413-418.